Research Square

Preprints are preliminary reports that have not undergone peer review.
They should not be considered conclusive, used to inform clinical practice,
or referenced by the media as validated information.

Generation of Supertoroidal Pulses with Controlled Topologies

Yijie Shen

yijie.shen@ntu.edu.sg

Nanyang Technological University https://orcid.org/0000-0002-6700-9902

Ren Wang

University of Electronic Science and Technology of China

Jinshan Cui

University of Electronic Science and Technology of China

Zeyi Zhang

University of Electronic Science and Technology of China

Yanhe Lyu

Nanyang Technological University

Junjie Shao

University of Electronic Science and Technology of China

Moran Zhang

University of Electronic Science and Technology of China

Sheng Liu

University of Electronic Science and Technology of China

Zixi Qiu

University of Electronic Science and Technology of China

Bing-Zhong Wang

University of Electronic Science and Technology of China

Mu-Sheng Liang

University of Electronic Science and Technology of China

Article

Keywords:

Posted Date: November 3rd, 2026

DOI: https://doi.org/10.21203/rs.3.rs-10251927/v1

License: This work is licensed under a Creative Commons Attribution 4.0 International License.
Read Full License

Additional Declarations: There is **NO** Competing Interest.

Generation of Supertoroidal Pulses with Controlled Topologies

Ren Wang[1,2*], Jinshan Cui[1], Zeyi Zhang[1], Yanhe Lyu[3,4], Junjie Shao[1*], Moran Zhang[1], Sheng Liu[1], Zixi Qiu[1], Bing-Zhong Wang[1], Mu-Sheng Liang[1*], Yijie Shen[3,4*]

[1] *Institute of Applied Physics, University of Electronic Science and Technology of China, Chengdu 611731, China*

[2] *Yangtze Delta Region Institute (Huzhou), University of Electronic Science and Technology of China, Huzhou 313098, China*

[3] *Centre for Disruptive Photonic Technologies, School of Physical and Mathematical Sciences, Nanyang Technological University, Singapore 637371, Singapore*

[4] *School of Electrical and Electronic Engineering, Nanyang Technological University, Singapore 639798, Singapore*

* E-mail: rwang@uestc.edu.cn (R.W.); msliang@uestc.edu.cn (M.S.L.); 909703671@qq.com (J.S.); yijie.shen@ntu.edu.sg (Y.S.)

Abstract

Toroidal electromagnetic excitations have been recognized as the third fundamental excitations besides classic electric and magnetic dipoles, offering great promise for next-generation information carriers. However, a big step ahead blocking the practical implementation remains the deterministic generation and control of the full family from toroidal to supertoroidal pulses with tailored topological orders. Here, we experimentally demonstrate supertoroidal pulse generation by both passive and active spatiotemporal metasurfaces. We also observe and manipulate their nontrivial properties—including fractal-like singularities, deep-subwavelength skyrmions, nondiffracting propagation, and space–time superoscillations—which were previously predicted but unrealized. These findings complete a missing chapter of supertoroidal electrodynamics and open immediate horizons for ultra-capacity robust communications and exotic light-matter interactions.

Introduction

In classical electromagnetism, fields are basically described through electric and magnetic multipole expansions, however, such framework is theoretically incomplete without the inclusion of a third kind of excitations, predicted by Zel′dovich in 1957 [1]. Such essential excitations were formally unveiled as toroidal multipoles, with further theoretical development mainly by Afanasiev [2], which were experimentally verified in 2010 [3,4]. Soon after, toroidal dipolar excitations in metamaterials enabled nonradiating anapoles [5–7] with advanced applications of scattering suppression [5–7], nanolaser dispersion engineering [8], atomic state transitions [9], etc., giving rise to a vibrant field of toroidal electrodynamics [10].

As a breakthrough in the past decade, the toroidal excitations were extended from matter to free space [11]. The free-space excitation was theoretically identified by Hellwarth and Nouchi in 1996 [12], while its experimental observation of toroidal light pulses was reported in 2022 [13], which subsequently sparked broader interest across optical, terahertz and microwave regimes [14–16]. The toroidal pulses have recently stimulated not only fundamental studies in high-dimensional structured light [17–19], quantum-like nonseparability [20–22], singular optics [23,24], spacetime optics [25,26], and topological resilience [15,27], but also promised applications of wireless super-resolution sensing [28–30] and nontrivial light-matter interactions [31–33].

However, these are only based on the elementary-order toroidal light pulse. The crucial challenge for practical use lies in controllably generating higher-order

topological excitations from toroidal pulses. Recent theories have revealed an extended family of toroidal pulses — supertoroidal pulses (STPs) — with the elementary toroidal pulse as the simplest member in which [34]. These pulses not only possess single-cycle toroidal topology and space-time nonseparability as the elementary holds, but also extensively predict a variety of intriguing and fundamentally nontrivial properties, such as order-driven fractal-like singularities [34], deep-subwavelength skyrmions [19,34], nondiffracting propagation [35], Kármán vortex streets [35], space–time superoscillations [36], and strongly longitudinal polarization [37]. Despite this rich theoretical landscape, STPs have remained experimentally inaccessible to date.

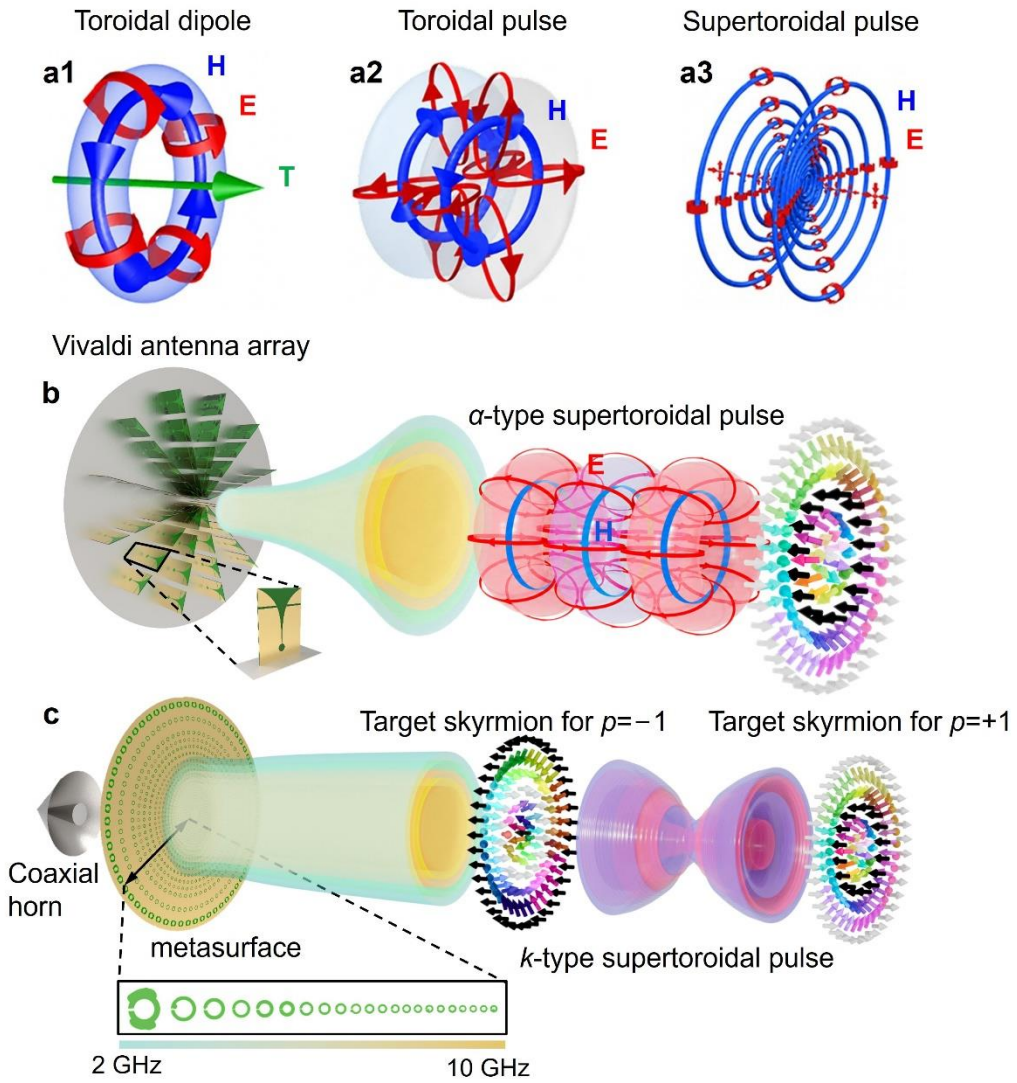
Here, we report the first experimentally controllable generation of supertoroidal pulses by both active and passive metasurfaces. The first employs an active metasurface—an ultrawideband concentric-ring Vivaldi antenna array—to directly radiate order-controlled STPs (α-type), while the second realizes generation of nondiffracting STPs (k-type) via the conversion of toroidal pulses using a metasurface with spatially distributed frequency-selective responses. Using these platforms, we experimentally characterize the spatiotemporal fields and spectral distributions of the generated STPs, revealing key features predicted by theory, including order-controlled skyrmion textures, Kármán vortex streets, strongly longitudinally polarized fields, nondiffracting propagation, and the first observation of space–time superoscillations. These findings provide a viable route for realizing higher-order toroidal excitations and open new opportunities for ultrafast spatiotemporal topologies and robust information transfers.

Results

Basic concepts for STPs.

STPs are space-time nonseparable solutions of Maxwell's equations, the field expressions of which can be derived from a scalar generating function $f \propto e^{-s/q_3} \Big/ \left[\left(q_1 + i\tau \right) \left(s + q_2 \right)^{\alpha} \right]$ with specific Hertz potential, as detailed in the Methods, according to Ziolkowski's "electromagnetic directed-energy pulse trains" theory [12,38,39]. In the generating function, q_1 and q_2 are evaluating pulse's effective wavelength and Rayleigh range, respectively, and α is a real parameter satisfying $\alpha \geqslant 1$ and ensuring localized finite energy. The elementary toroidal pulses are subject to α=1 and $q_3 \to \infty$, which show toroidal field structures akin to toroidal dipoles (Fig. 1**a1**) but as propagating pulses in free space (Fig. 1**a2**). STPs are generalized solutions driven by non-unity values of α and giving rise to higher-order nested toroidal topologies (Fig. 1**a3**). By varying the order α, the α-type STPs can support a variety of skyrmion textures [34] and host space–time superoscillations [36], in which the topologically featured field locally oscillates faster than the highest Fourier component in its spectrum.

The STPs can be further generalized by introducing finite value of q_3 (or k=1/q_3 [37, 40], as detailed in the Methods) which evaluate a pulse's transverse divergent X-shaped structure to counterbalance the longitudinal divergence thus towards nondiffraction. The k-type STPs can exhibit strong longitudinal polarization [37], nondiffracting propagation of arbitrarily long distance [35], as well as exotic topology of Kármán vortex streets [35].



96

97 **Fig. 1. Generation schemes for STPs.** (**a**) Comparison of toroidal dipole **T** in materials,
98 toroidal pulses and STPs in free space. STPs exhibit higher-order toroidal structures,
99 giving rise to a range of nontrivial phenomena, including deep-subwavelength
100 skyrmions of various orders, nondiffracting propagation, Kármán vortex streets, space–
101 time superoscillations, and strongly longitudinal polarization. (**b**) Direct radiation of α-
102 type STPs using an ultrawideband concentric-ring Vivaldi antenna array. All antenna
103 elements are radially polarized and arranged every 30° along the azimuth, with 12
104 elements per ring. The order α is determined by the number of array rings; arrays with
105 1, 2, 3, and 4 rings of elements correspond to α = 2, 4, 6, and 8, respectively. (**c**)

Emission of *k*-type STPs from a metasurface with spatially distributed frequency-selective functionality, excited by a toroidal pulse generator—a coaxial horn antenna. The metasurface has a radius of 0.5 m, and the distance between the coaxial horn and the metasurface is 0.5 m. An enlarged view of the unit cells along one radius of the metasurface is included in the figure. The green patterns represent etched slots in the copper foil on the substrate. Each unit cell exhibits a distinct transmission frequency; the unit cell size gradually increases from the inner to the outer rings, with the operating frequency decreasing from approximately 10 GHz to around 2 GHz.

Generation schemes for STPs.

Hereinafter, meta-integrated generators for both α-type and *k*-type STPs are designed. The α-type STPs are directly radiated by an ultrawideband concentric-ring Vivaldi antenna array, where the order α is determined by the number of array rings. The *k*-type STPs are produced by launching toroidal pulses into a metasurface with spatially distributed frequency-selective properties.

To generate α-type STPs, a concentric-ring Vivaldi antenna array is used, as shown in Fig. 1**b**. All antenna elements are radially polarized to match the transverse polarization of STPs. According to Gauss's law, purely radial polarization cannot exist independently along the propagation axis, so the array naturally produces the longitudinal polarization component required for STPs. Each antenna element is identical and possesses ultrawideband characteristics, spanning approximately 2–10 GHz, thereby meeting the broad spectral requirements of STPs, as detailed in the Supplementary Material. The elements are arranged every 30° along the azimuth, with

12 per ring. Because the frequency bands of all elements overlap, radiation from different rings and interference beyond the aperture, producing interference fringes in the spectral domain. These fringes form the multiple curved stripe patterns characteristic of STPs. As the number of rings increases, the number of spectral fringes also grows, corresponding to different orders of α-type STPs, as illustrated in Fig. 2. Specifically, arrays with 1, 2, 3, and 4 rings correspond to $\alpha = 2$, 4, 6, and 8, respectively.

To generate *k*-type STPs, toroidal pulses are passed through a metasurface with spatially distributed frequency-selective functionality, as shown in Fig. 1**c**. The toroidal pulse generator is a coaxial horn antenna. Detailed structural parameters and performances for the coaxial horn antenna can be found in Supplementary Materials and [15]. The metasurface features a rotationally symmetric arrangement composed of multiple concentric frequency-selective unit cells. It is specifically designed to manipulate the transverse polarization component, with each concentric ring of unit cells exhibiting distinct transmission frequencies for transverse polarization. From the inner to the outer rings, unit cell dimensions gradually increase, resulting in the central resonance frequency of elementary mode decreasing from approximately 10 GHz to around 2 GHz. Each unit cell is designed based on an open resonant ring using topology optimization algorithms; further details are provided in the Supplementary Materials. The elementary-mode transmission bands of several adjacent unit cells partially overlap. In addition, the transmission frequencies of higher-order modes in the outer-ring unit cells overlap with the elementary-mode transmission frequencies of the inner-ring unit cells. As a result, the transmission spectra of the different unit cells undergo diffraction

and interference after passing through the metasurface, forming the curved stripe pattern required for generating STPs. In addition to reshaping the spectral distribution, the metasurface also suppresses the transmitted transverse polarization component. This occurs because each ring of the metasurface transmits only a portion of the transverse polarization frequencies, thereby allowing the longitudinal component to dominate after transmission, consistent with the *k*-type STPs that are characterized by enhanced longitudinal polarization [37]. As will be shown later, the ratio of longitudinally to transversely polarized field components increases substantially after transmission compared to that of the original toroidal pulse.

Observation of *α*-type STPs.

The space–time electric field distributions of the STPs are shown in Fig. 2**a**. Both the number of lobes and the number of singularities (including vortices and saddle points) increase with the order α. The overall view of the field distributions and their zero contours is presented in the Supplementary Materials to more clearly illustrate the locations of the singularities and the fractal structure of the field distribution. On transverse cross-sections near the singularities, the electric fields exhibit skyrmion textures, as shown in Fig. 2**b**. With increasing α, both the theoretical and measured skyrmion textures evolve into higher-order target skyrmions, appearing as progressively nested skyrmion textures. The measurements were carried out in a microwave anechoic chamber. Rectangular horn probes and monopole probes were used to detect the transversely and longitudinally polarized electric fields, respectively;

171 further details are provided in the Methods section and Supplementary Materials.
172 Owing to the alternating parity of the lobe number with increasing α, the skyrmion
173 number of the target skyrmions on the transverse cross-sections alternates between
174 approximately 0 and 1, in agreement between theories and measurements, confirming
175 the generation of well-defined target skyrmions. Details of the skyrmion number
176 calculation are provided in the Supplementary Materials. This behavior is consistent
177 with the predictions of Ref. [34].

178 Spectral distributions of the theoretical and experimentally generated α-type STPs
179 are shown in Fig. 2**c**. Since the generation scheme does not precisely control the spectral
180 distribution at each spatial point to exactly match the ideal supertoroidal pulse spectrum,
181 but rather uses natural diffraction and interference of transmitted spectral components
182 to form the stripe-like spectral distribution, the measured results exhibit stripe patterns
183 characteristic of STPs but differ slightly from the theoretical case. Nevertheless, both
184 the theoretical and experimental spectra feature multiple curved stripe patterns. With
185 increasing α, the number of spectral lobes in the theoretical STPs increases;
186 correspondingly, as the number of Vivaldi antenna rings in the array increases, the
187 measured spectra also exhibit more lobes. Theoretical results show that the number of
188 spectral sidelobes is the same for α=3 and 4, 5 and 6, and 7 and 8 (see Supplementary
189 Materials). Therefore, only the cases of α=2, 4, 6, and 8 are presented here. The spectra
190 generated by arrays of 1, 2, 3, and 4 rings of Vivaldi antenna elements correspond well
191 to the theoretical spectra for α = 2, 4, 6, and 8, respectively. In the measured results with
192 four array rings, the spectra display spurious speckles arising from complex

interference and measurement errors—the latter having a stronger impact on the smaller sidelobes generated by interference. Nevertheless, compared with the three-ring case, the spectra still reveal the appearance of additional minor sidelobes. The longitudinally polarized component exhibits a variation trend similar to that of the transversely polarized component shown in Fig. 2**c**; however, the transverse component vanishes along the propagation axis (ρ = 0), where the longitudinal component reaches its maximum. Details are provided in the Supplementary Material.

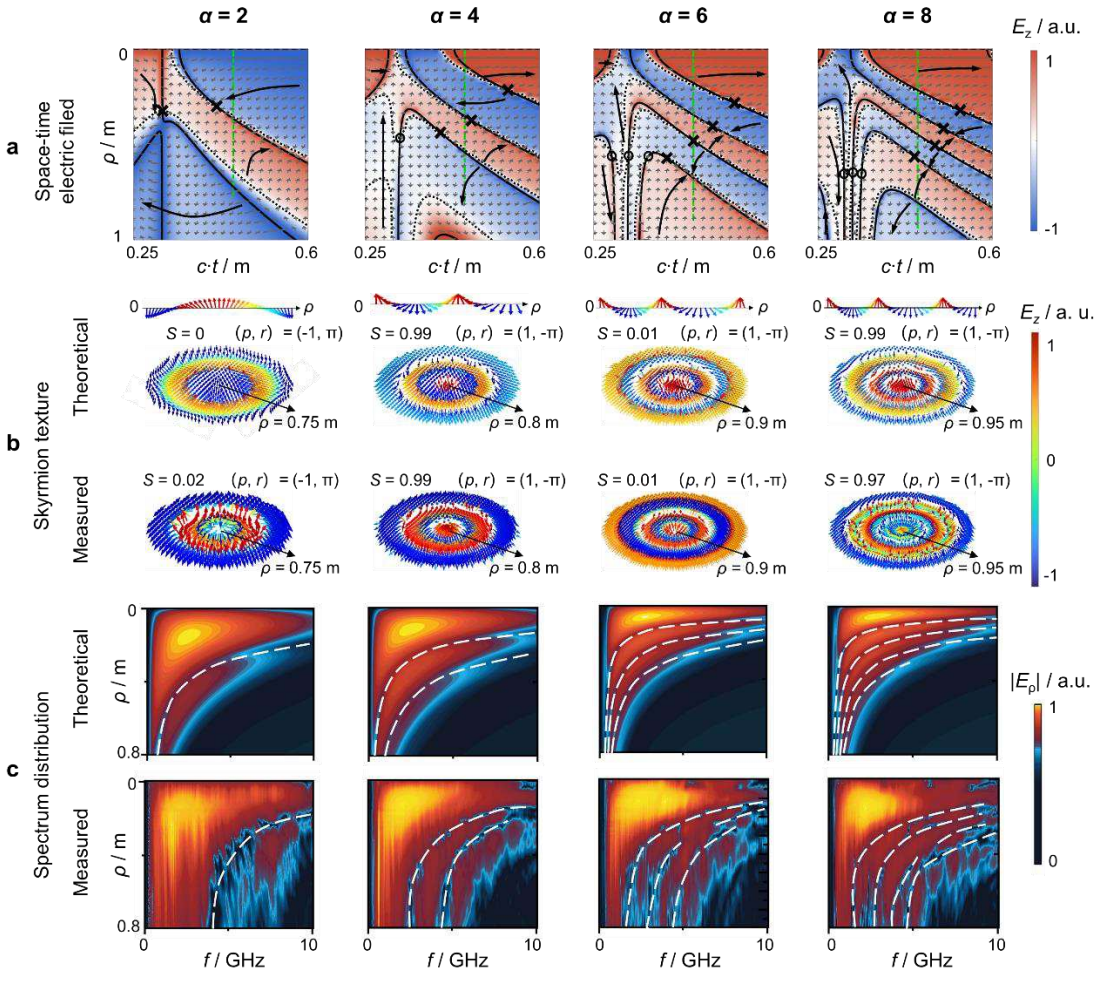


Fig. 2. Space–time electric fields, skyrmion textures, and spectrum distributions of α-type STPs. (**a**) Space–time electric field distributions of STPs with α=2, 4, 6, and 8. ○ and × denote the centers of vortices and saddle points, respectively, while the black

solid and dash curves represent the zero contours of the transverse and longitudinal polarization components, respectively. All the number of lobes, vortices, saddle points, and zero contours increase with α. On transverse cross-sections near saddle points, the electric fields exhibit skyrmion textures. (**b**) Theoretical and measured skyrmion textures, taken at z=0.32 m and t=1.5 ns, corresponding to the green dashed lines in (**a**). With increasing α, both theoretical and measured textures evolve into higher-order target skyrmions, forming progressively nested structures. The skyrmion number S, evaluated on transverse cross-sections within ρ<0.8 m, alternates between approximately 0 and 1. The theoretical predictions and experimental measurements are in good agreement, confirming the generation of well-defined target skyrmions. (**c**) Theoretical and measured spectra of the transverse polarization components, which vanish along the propagation axis (ρ=0). As the order α increases, the spectra develop additional lobes.

The transversely polarized electric fields of the STPs exhibit space–time superoscillation phenomena [36], as shown in Fig. 3. Superoscillation refers to the local oscillation of electromagnetic waves at rates exceeding the highest Fourier component of their spectrum [41]. To induce space-time superoscillations, a truncated spectrum is required. In both theoretical and measured cases, the spectral components of the STPs below 8 GHz were selected, and the corresponding space–time electric fields were obtained via inverse Fourier transform of the truncated spectra. As seen in Fig. 3, the field-line evolution trends of theoretical and measured STPs are in good agreement for all cases of α=2, 4, 6, and 8. For the transverse component, no clear superoscillation is

observed at α=2 or 4. At α=6 or 8, spatial oscillations finer than the wavelength of the highest Fourier component appear away from the propagation axis, indicating spatial superoscillations. These results indicate that for smaller α, spatial superoscillations are absent, whereas at larger α, the spatial superoscillations appear.

Ref. [36] theoretically predicts that, unlike spatial superoscillations occurring at tightly focused beam locations, STPs exhibit temporal superoscillations at the same positions where spatial superoscillations arise, resulting in space–time superoscillations. Accordingly, the time-domain signals at the spatial superoscillation locations were examined, the space–time superoscillationas for the case of α=8 are shown in Figs. 3b. Around ρ=0.09 m and t=1.75 ns, the theoretical spatiotemporal field exhibits superoscillatory behavior simultaneously in space and time, i.e., space–time superoscillations. Although device imperfections lead to slight mismatches between theory and experiment in the exact positions and times at which these effects appear, the experimental and theoretical results exhibit similar trends, confirming the observation of space–time superoscillations. The space–time superoscillations also exist in the case of α=6 (see the Supplementary Materials for details). Ref. [36] only theoretically predicted the existence of space–time superoscillations in the transversely polarized component of STPs. Interestingly, space–time superoscillations are also observed in the longitudinally polarized component of the STPs, as detailed in the Supplementary Materials.

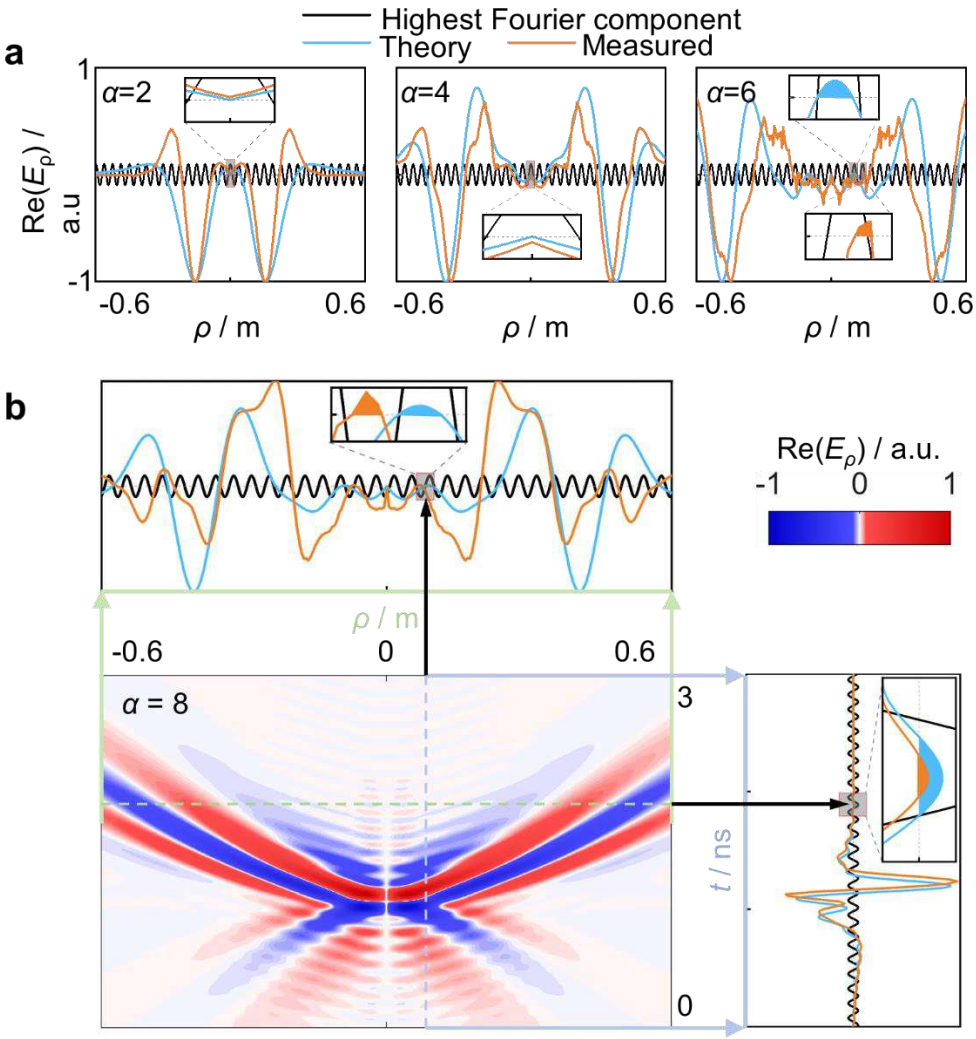


Fig. 3. Space-time superoscillation of *α*-type STPs. (**a**) Transversely polarized electric fields at z=0.32 m for α=2, 4, and 6, repectively. Both theoretical and measured STPs share the same highest frequency of 8 GHz, and their field-line evolution trends agree well. The gray curve in the figure represents an 8-GHz sinusoidal wave with a wavelength of 3.75 cm. The horizontal axis spans 32 wavelengths at 8 GHz, corresponding to a total length of 1.2 m. Neither the theoretical nor measured fields exhibit a clear superoscillation phenomenon at α=2 or 4. As α further increases, spatial oscillations smaller than the wavelength corresponding to the highest Fourier component emerge away from the propagation axis, revealing superoscillations. (**b**)

Space-time superoscillation at z=0.32 m for the case of α=8. In the two-dimensional spatiotemporal field distribution, many pronounced side lobes can be observed near ρ=0; their spatial and temporal periods are both much smaller than those of the main lobes. Around ρ=0.09 m and t=1.75 ns (see the enlarged inset dash lines), the theoretical spatiotemporal field exhibits superoscillatory behavior simultaneously in space and time, i.e., space–time superoscillations. In the measurements, space–time superoscillations are observed at approximately ρ=0.07 m and t=1.75 ns. Overall, the experimental and theoretical results show good agreement, confirming the observation of space–time superoscillations.

Observation of *k*-type STPs.

Using the setup illustrated in Fig. 1**c**, the generated *k*-type STPs are shown in Fig. 4. The three-dimensional (3D) spatiotemporal structure of the longitudinally polarized electric-field component exhibits a double-cone shape with multiple nested lobes, while the cross-section displays an X-shaped pattern. Theoretical investigations in [35] showed that the field distribution of STPs resembles a vortex street—a pattern of staggered swirling vortices commonly observed in fluid and gas dynamics that can propagate stably forward [42]. This vortex street distribution is experimentally observed in the generated *k*-type STPs, as illustrated in Fig. 4**b**. In the electric-field vector distribution in the longitudinal cross-section, multiple saddle points are continuously distributed along the propagation axis (ρ=0). On both sides of the axis, the electric field forms connected vortex rings, collectively producing a vortex-street pattern. The spatiotemporal structure and the vortex-street field distribution are

consistent with the theoretical predictions reported in Ref. [35].

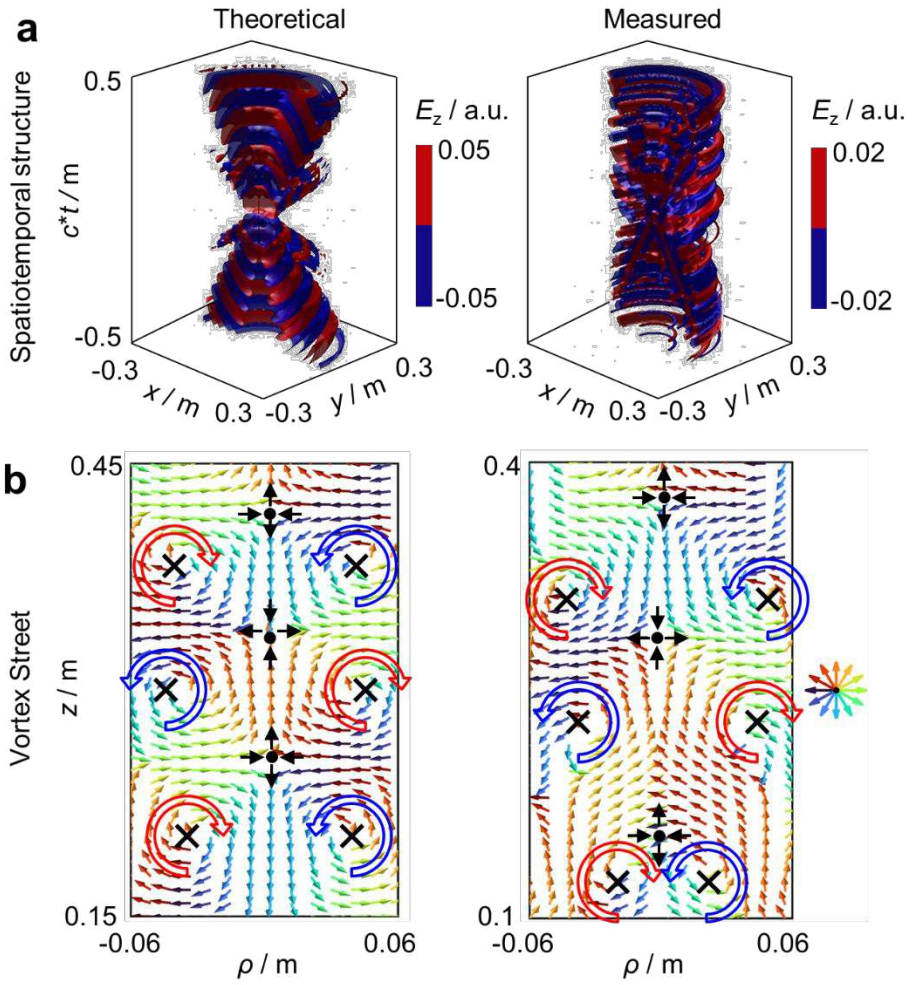


Fig. 4. Spatiotemporal structure and vortex street of *k*-type STPs. (**a**) 3D spatiotemporal structure of the longitudinally polarized electric-field component. Half of the 3D spatiotemporal field is shown to reveal the longitudinal cross-sectional profile. The overall structure exhibits a double-cone shape with multiple nested lobes, while the cross-section displays an X-shaped pattern. Although the measured spatiotemporal field contains several irregular small lobes and appears somewhat less ordered, the overall morphology and the X-shaped cross-sectional distribution are consistent with the theoretical prediction. (**b**) Vortex-street-like field distribution in the longitudinal cross-

section. Multiple saddle points are continuously distributed along the propagation axis (ρ=0). On both sides of the axis, the electric field forms connected vortex rings, collectively producing a vortex-street pattern. The measured field distribution agrees well with the theoretical results. Near adjacent vortex rings in the vortex-street pattern, oppositely oriented skyrmions appear, as shown in the Supplementary Materials.

Fig. 5 compares the propagation of both theoretical and measured STPs with that of toroidal pulses. Fig. 5**a** shows the maximum electric field amplitude at each position during propagation for the toroidal and STPs, respectively, both emitted from apertures of identical size. The measured toroidal pulses were obtained through experimental measurements of the coaxial horn antenna. As shown in Fig. 5**a**, the electric field of toroidal pulses mainly distributes on either side of the propagation axis and gradually diverges outward. In contrast, the STPs' fields concentrate near the propagation axis with minimal divergence. The angular spans of the 1 dB outer contours for the toroidal pulses are 15.54° and 23.02° in theory and experiment, respectively. In contrast, those for the STPs are only 1.84° and 2.14°, respectively, which are much smaller than in the toroidal-pulse case. The evolution of the pulse width at half maximum in the transverse direction during propagation is plotted for both pulse types in Fig. 5**b**. The results indicate a clear increase in pulse width for toroidal pulses, whereas the STPs maintain nearly constant pulse width throughout propagation. The trends in theoretical and measured results show strong agreement.

The longitudinal and transverse polarization components of pulses with toroidal

structures predominantly occupy the propagation axis and its sides, respectively. Fig. 5**a** reveals that the total field of toroidal pulses mainly resides off-axis, while that of STPs concentrates on-axis, indicating the dominance of transverse and longitudinal polarization components in toroidal and STPs, respectively. To further clarify this, the ratio of the maximum longitudinal to transverse polarization components at various propagation distances is plotted in Fig. 5**c**. For measured toroidal pulses, this ratio remains below 0.5 and decreases slowly; for theoretical toroidal pulses, it stays below 0.15 with a similar decreasing trend. In all cases, the transverse component dominates throughout propagation. In contrast, near the emission aperture (the metasurface in Fig. 1), STPs exhibit a longitudinal-to-transverse polarization ratio of approximately 4–6, indicating that the metasurface effectively suppresses the transverse component of the toroidal pulse. Away from the aperture, this ratio decreases rapidly, reaching about 1 at a propagation distance of approximately 0.5 m and then stabilizing. These results confirm that, despite the use of a finite emission aperture, the generated STPs maintain a significantly stronger longitudinal field component than toroidal pulses.

Interestingly, similar to the α-type STPs, the k-type pulses also display superoscillations and diverse skyrmion textures. Further details are provided in the Supplementary Materials.

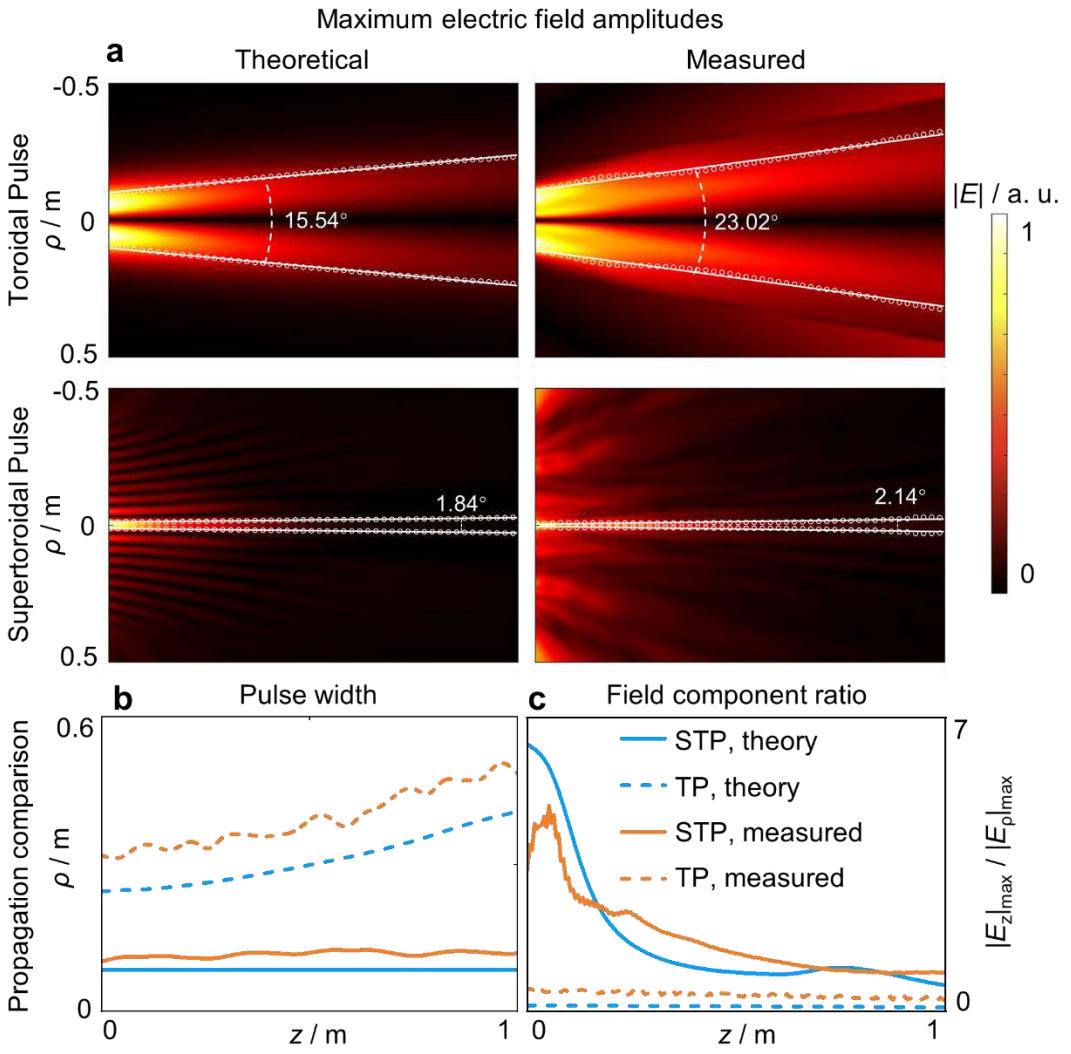


Fig. 5. Nondiffraction and strong longitudinal polarization of *k*-type STPs. (**a**) Maximum electric field amplitudes at each spatial position during propagation for toroidal pulses and STPs, respectively, both emitted from apertures of identical size. The electric field of toroidal pulses primarily distributes on either side of the propagation axis and gradually diverges outward, whereas the STPs' field is concentrated near the propagation axis with minimal divergence. The white circles and fitted curves in the figure represent the outer contour at each z position where the field magnitude decreases by 1 dB relative to the maximum at that specific z. The angular spans of the 1 dB outer contours for the toroidal pulses are 15.54° and 23.02° in theory

and experiment, respectively. In contrast, those for the STPs are only 1.84° and 2.14°, respectively, which are much smaller than in the toroidal-pulse case. (**b**) Evolution of the pulse width at half maximum in the transverse direction during propagation for both toroidal pulses and STPs. The pulse width of toroidal pulses increases noticeably, while that of STPs remains nearly constant. TP: toroidal pulse. (**c**) Ratio of the maximum longitudinal to transverse polarization components for toroidal and STPs. The transverse component dominates throughout propagation in toroidal pulses. Near the emission aperture, STPs exhibit a longitudinal component 4 to 6 times stronger than the transverse component; this ratio stabilizes near 1 beyond the aperture.

Discussions

This work demonstrates the generation of STPs and provides experimental evidence of several theoretically predicted features, including skyrmion textures, vortex streets, strong longitudinal polarization, nondiffracting propagation, and space–time superoscillations.

Given that toroidal pulse generators have already been realized at optical and terahertz frequencies, and that metasurfaces with spatially distributed frequency-selective responses can be engineered in these regimes, the approach proposed here offers a viable route toward extending STP generation to optical and terahertz domains.

The observed characteristics of STPs open up opportunities across a range of applications. Their diverse skyrmion textures provide new degrees of freedom for topology-rich information encoding. Nondiffracting propagation enables the robust

long-distance transmission of information encoded in these topological features, which is crucial for communication applications based on supertoroidal pulses. Strong longitudinal polarization introduces an additional degree of freedom beyond the two transverse polarizations employed in conventional communication systems, suggesting the potential for high-capacity wireless channels with three independent polarization states.

Moreover, because existing stealth and detection schemes are primarily designed for transversely polarized fields, the strong longitudinal components of supertoroidal pulses may offer new opportunities for counter-stealth detection. The first observation of space–time superoscillations may also enable Fourier-limit-exceeding super-resolution localization, with potential applications in metrology, ultrafast spectroscopy, and microscopy. In addition, controllable space–frequency stripes could facilitate spatiotemporal field shaping, while spatiotemporal vortex streets may enable topological field transport.

Methods

Theoretical analysis method. STPs are derived from a class of solutions to the homogeneous free-space wave equation, termed electromagnetic directed energy pulse trains [38–40]:

$$f\left(\rho,z,t\right)=\frac{1}{4\pi\mathrm{i}\left(q_1+\mathrm{i}\tau\right)}\int_0^\infty F\left(k\right)e^{-ks(\rho,z,t)}dk \tag{1}$$

where q_1 a real, positive, adjustable parameter with units of length,

$s(\rho,z,t)=\frac{\rho^2}{q_1+\mathrm{i}\tau}-\mathrm{i}\sigma$, $\rho^2=x^2+y^2$, $\tau=z-\mathrm{c}t$, and $\sigma=z+\mathrm{c}t$. This representation employs basis functions that are spatially localized and suited for describing the directed transfer of electromagnetic energy through space. The resulting pulses possess finite energy when $F(k)$ is square-integrable. By designing different forms of $F(k)$, various scalar wave functions can be obtained from Eq. (1), enabling the construction of localized electromagnetic pulses with distinct characteristics.

One particularly notable choice of $F(k)$ in Eq. (1) is the modified power spectrum, which yields the modified power-spectrum pulse [12, 40]:

$$f=f_0\frac{e^{-s/q_3}}{(q_1+i\tau)(s+q_2)^{\alpha}} \tag{2}$$

Here, q_1, q_2, and q_3 are real, positive, adjustable parameters with units of length. The real, dimensionless parameter α must satisfy $\alpha\geq1$ to ensure that the electromagnetic pulse has finite energy. Without loss of generality, f_0 is taken as a real constant. By setting $q_1 \square q_2$, $\alpha=1$, and $q_3\to\infty$, toroidal pulses can be obtained, where q_1 characterizes the wavelength of these pulses and q_2 represents the "Rayleigh range" or the depth of the focal region.

An extended family of such pulses—referred to as STPs—can be theoretically investigated using the general solution for values of $\alpha>1$ [34]. In this work, these are termed α-type STPs. In 2024, the q_3-type STPs were introduced as another extended family of toroidal pulses capable of propagating without diffraction [35]. For α-type STPs, q_3 is taken to be infinite. As the finite q_3 value in Eq. (2) decreases, the

longitudinal divergence of the pulse tends to diminish; when q_3=q_1, the pulse becomes nondiffracting.

In 2004, Lekner noted that the integral in Eq. (1) can be expressed as a function $f(s)$ for each chosen $F(k)$ [40], allowing Eq. (1) to be rewritten as

$$f(\rho,z,t)=\frac{f(s)}{4\pi\mathrm{i}(q_1+\mathrm{i}\tau)}. \tag{3}$$

Let $f(s)=e^{-ks}/(s+q_2)$, which yields a new scalar wave function—referred to as the oscillatory wave function [40]. In [37], the oscillatory wave function with nonzero k was examined, leading to the introduction of a third type of supertoroidal pulse, termed the k-type supertoroidal pulse, characterized by a strongly longitudinally polarized field component. Comparison with Eq. (2) reveals that k-type STPs are equivalent to q_3-type STPs. The case k =q_1 corresponds to q_3 =q_1, implying that the resulting STPs should exhibit nondiffraction and strong longitudinal polarization—predictions that will be experimentally verified later in this work. Furthermore, when k=0, q_3 becomes infinite, and Eq. (3) reduces to the scalar generating function of the toroidal pulse.

Using the scalar wave function described above, both the electric and magnetic fields of a pulse can be constructed. For transverse electric (TE) pulses based on the scalar wave function, the electric and magnetic fields are expressed as $\boldsymbol{E}=-\mu_0\partial_t\boldsymbol{A}$ and $\boldsymbol{B}=\mu_0\nabla\times\boldsymbol{A}$, where $\boldsymbol{A}$ denotes the vector potential. Transverse magnetic (TM) pulses can be obtained from TE pulses via the dual transformation $\boldsymbol{E}\to c\nabla\times\boldsymbol{A}$, $\boldsymbol{B}\to -c^{-1}\partial_t\boldsymbol{A}$. Different pulse forms can be derived by employing different vector

potentials.

In this paper, both α-type and k-type STPs, associated with the vector potential $\boldsymbol{A} = \nabla \times [0, 0, f]$, were generated. The theoretical results of α-type STPs were calculated using Eq. (2) with parameters q_1=0.01m, q_2=50q_1, and $q_2 \to \infty$. The theoretical results of k-type STPs were computed using Eq. (3) with parameters q_1=0.01m, q_2=50q_1, and k=q_1. The theoretical toroidal pulses are calculated from Eq. (3) with parameters q_1=0.01m, q_2=50q_1, and k=0. According to Ref. [37], when k =q_1, the supertoroidal pulse exhibits strong longitudinal polarization. The case k =q_1 corresponds to q_3 =q_1, implying that the resulting STPs should exhibit nondiffraction [35].

Measurement method. A microwave anechoic chamber was used to measure the electromagnetic fields of the generated STPs. For α-type STPs, the receiving antenna was the Vivaldi array connected through a divider system; for k-type pulses, the receiving antenna was the toroidal pulse generator, i.e., a coaxial horn antenna, purposely designed to produce toroidal pulses with parameters q_1=0.01m and q_2=50q_1. In both cases, standard rectangular horn probes and monopole probes were used as transmitting antennas to measure the transverse and longitudinal polarization components, respectively. The probes were mounted on scanning rails, allowing three-dimensional movement controlled by the measurement system. For k-type measurements, the metasurface and coaxial horn were aligned coaxially with a fixed separation of 0.5 m, while the probe-to-device distance was adjustable to sample fields at different positions. For α-type measurements, the probes could also scan radially

across the Vivaldi array to map spectral distributions. A vector network analyzer connected to the probes and coaxial horn measured the S_{21} parameter to obtain the magnitude and phase of the electromagnetic field at different spatial positions. Time-domain experimental results were retrieved by applying an inverse Fourier transform to the measured spatial magnitudes and phases. By combining the transverse and longitudinal polarization components, the full spatiotemporal vector field distribution was reconstructed, facilitating the observation of topological textures.

References

[1] Ia. B. Zel'dovich, Electromagnetic interaction with parity violation, *Sov. Phys. JETP* **6**, 1184 (1958).

[2] Afanasiev, G. N., & Stepanovsky, Y. P. The electromagnetic field of elementary time-dependent toroidal sources. *J. Phys. A: Math. Gen.* **28**(16), 4565 (1995).

[3] Kaelberer, T., Fedotov, V. A., Papasimakis, N., Tsai, D. P., & Zheludev, N. I. Toroidal dipolar response in a metamaterial. *Science* **330**(6010), 1510–1512 (2010).

[4] Basharin, A. A., Kafesaki, M., Economou, E. N., Soukoulis, C. M., Fedotov, V. A., Savinov, V., & Zheludev, N. I. Dielectric metamaterials with toroidal dipolar response. *Phys. Rev. X* **5**(1), 011036 (2015).

[5] Ballantine, K. E., & Ruostekoski, J. Radiative toroidal dipole and anapole excitations in collectively responding arrays of atoms. *Phys. Rev. Lett.* **125**(6), 063201 (2020).

[6] Yang, B., Bi, Y., Zhang, R. X., Zhang, R. Y., You, O., Zhu, Z., ... & Zhang, S. Momentum space toroidal moment in a photonic metamaterial. *Nat. Commun.*

12(1), 1784 (2021).

[7] Miroshnichenko, A. E., Evlyukhin, A. B., Yu, Y. F., Bakker, R. M., Chipouline, A., Kuznetsov, A. I., ... & Kivshar, Y. S. Nonradiating anapole modes in dielectric nanoparticles. *Nat. Commun.* **6**(1), 8069 (2015).

[8] Totero Gongora, J. S., Miroshnichenko, A. E., Kivshar, Y. S., & Fratalocchi, A. Anapole nanolasers for mode-locking and ultrafast pulse generation. *Nat. Commun.* **8**(1), 15535 (2017).

[9] Kuprov, I., Wilkowski, D., & Zheludev, N. Toroidal optical transitions in hydrogen-like atoms. *Sci. Adv.* **8**(45), eabq6751 (2022).

[10] Zheludev, N. I., & Wilkowski, D. The rise of toroidal electrodynamics and spectroscopy. *ACS Photonics*, **10**(3), 556–558 (2023).

[11] Papasimakis, N., Fedotov, V. A., Savinov, V., Raybould, T. A., & Zheludev, N. I. Electromagnetic toroidal excitations in matter and free space. *Nat. Mater.* **15**(3), 263–271 (2016).

[12] Hellwarth, R. W., & Nouchi, P. Focused one-cycle electromagnetic pulses. *Phys. Rev. E* **54**(1), 889 (1996).

[13] Zdagkas, A., McDonnell, C., Deng, J., Shen, Y., Li, G., Ellenbogen, T., ... & Zheludev, N. I. Observation of toroidal pulses of light. *Nat. Photon.* **16**(7), 523–528 (2022).

[14] Jana, K., Mi, Y., Møller, S. H., Ko, D. H., Gholam-Mirzaei, S., Abdollahpour, D., ... & Corkum, P. B. Quantum control of flying doughnut terahertz pulses. *Sci. Adv.* **10**(2), eadl1803 (2024).

[15] Wang, R., Bao, P.-Y., Hu, Z.-Q., Shi, S., Wang, B.-Z., Zheludev, N. I., & Shen, Y. Observation of resilient propagation and free-space skyrmions in toroidal electromagnetic pulses, *Appl. Phys. Rev.* **11**, 031411 (2024).

[16] Niu, L., Feng, X., Zhang, X., Yu, W., Wang, Q., Lang, Y., Xu, Q., Chen, X., Ma, J., Qiu, H., Shen, Y., Zhang, W., & Han, J. Electric-magnetic-switchable free-space skyrmions in toroidal light pulses via a nonlinear metasurface, *Optica* **13**, 203 (2026).

[17] Wang, R., Ying, B., Shi, S., Wang, J., Wang, B. Z., Liang, M., & Shen, Y. Hybrid electromagnetic toroidal vortices. *Sci. Adv.* **11**(8), eads4797 (2025).

[18] He, C., Shen, Y., & Forbes, A. Towards higher-dimensional structured light. *Light Sci. Appl.* **11**(1), 205 (2022).

[19] Shen, Y., Zhang, Q., Shi, P., Du, L., Yuan, X., & Zayats, A. V. Optical skyrmions and other topological quasiparticles of light. *Nat. Photon.* **18**(1), 15–25 (2024).

[20] Shen, Y., Zdagkas, A., Papasimakis, N., & Zheludev, N. I. Measures of space-time nonseparability of electromagnetic pulses. *Phys. Rev. Res.* **3**(1), 013236 (2021).

[21] Shen, Y., Nape, I., Yang, X., Fu, X., Gong, M., Naidoo, D., & Forbes, A. Creation and control of high-dimensional multi-partite classically entangled light. *Light Sci. Appl.* **10**(1), 50 (2021).

[22] Shen, Y., & Rosales-Guzmán, C. Nonseparable states of light: from quantum to classical. *Laser Photon. Rev.* **16**(7), 2100533 (2022).

[23] Zdagkas, A., Papasimakis, N., Savinov, V., Dennis, M. R., & Zheludev, N. I. Singularities in the flying electromagnetic doughnuts. *Nanophotonics* **8**(8), 1379–

505 1385 (2019).
506 [24] Shi, S., Wang, R., Xiong, M., Zhou, Q., Wang, B. Z., & Shen, Y. Double-helix
507 singularity and vortex–antivortex annihilation in space-time helical
508 pulses. *Nanophotonics* **14**(6), 741–747 (2025).
509 [25] Chen, W., Liu, Y., & Lu, Y. Q. Spatiotemporal optical vortices: Toward tailoring
510 orbital angular momentum of light in full space-time. *ACS Photonics* **10**(7), 2011–
511 2019 (2023).
512 [26] Yessenov, M., Hall, L. A., Schepler, K. L., & Abouraddy, A. F. Space-time wave
513 packets. *Adv. Opt. Photon.* **14**(3), 455–570 (2022).
514 [27] Shen, Y., Pidishety, S., Nape, I., & Dudley, A. Self-healing of structured light: a
515 review. *J. Optics* **24**(10), 103001 (2022).
516 [28] Wang, R., Bao, P. Y., Feng, X., Wu, J., Wang, B. Z., & Shen, Y. Single-antenna
517 super-resolution positioning with nonseparable toroidal pulses. *Commun.*
518 *Phys.* **7**(1), 356 (2024).
519 [29] Wan, Z., Wang, H., Liu, Q., Fu, X., & Shen, Y. Ultra-degree-of-freedom structured
520 light for ultracapacity information carriers. *ACS Photonics* **10**(7), 2149–2164
521 (2023).
522 [30] Chen, L., Li, X. Y., Shen, Y., Gu, Z., Su, J. L., Xiao, Q., ... & Cui, T. J.
523 Programmable skyrmions for communication and sensing. *Nat. Electron.* **9**, 479–
524 488 (2026).
525 [31] Zhu, L., Tai, Y., Li, H., Hu, H., Li, X., Cai, Y., & Shen, Y. Multidimensional optical
526 tweezers synthetized by rigid-body emulated structured light. *Photonics Res.* **11**(9),

1524–1534 (2023).

[32] Wang, L., Lacoste, C., Corkum, P., Brabec, T., & Chang, Z. Toroidal pulse enhanced XUV generation. arXiv:2605.31428 (2026).

[33] Raybould, T., Fedotov, V. A., Papasimakis, N., Youngs, I., & Zheludev, N. I. Exciting dynamic anapoles with electromagnetic doughnut pulses. *Appl. Phys. Lett.* **111**(8), 081104 (2017).

[34] Shen, Y., Hou, Y., Papasimakis, N., & Zheludev, N. I. Supertoroidal light pulses as electromagnetic skyrmions propagating in free space. *Nat. Commun.* **12**(1), 5891 (2021).

[35] Shen, Y., Papasimakis, N., & Zheludev, N. I. Nondiffracting supertoroidal pulses and optical "Kármán vortex streets". *Nat. Commun.* **15**(1), 4863 (2024).

[36] Shen, Y., Papasimakis, N., & Zheludev, N. I. Space-time superoscillations. *Nat. Commun.* **17**(1), 2053 (2026).

[37] Wang, R., Yang, D. T., Xin, T., Shi, S., Wang, B. Z., & Shen, Y. Optical atompilz: propagation-invariant strongly longitudinally polarized toroidal pulses. *Appl. Phys. Lett.* **125**(11), 111101 (2024).

[38] Ziolkowski, R. W. Exact solutions of the wave equation with complex source locations. *J. Math. Phys.* **26**(4), 861–863 (1985).

[49] Ziolkowski, R. W. Localized transmission of electromagnetic energy. *Phys. Rev. A* **39**(4), 2005 (1989).

[40] Lekner, J. Angular momentum of electromagnetic pulses. *J. Opt. A: Pure Appl. Opt.* **6**(3), S128 (2004).

[41] Zheludev, N. I., & Yuan, G. Optical superoscillation technologies beyond the diffraction limit. *Nat. Rev. Phys.* **4**(1), 16–32 (2022).

[42] von Kármán, T. *Aerodynamics. Selected topics in the light of their historical development*. Cambridge University Press (1954).

Acknowledgments

This work has been supported by the National Natural Science Foundation of China (U2341207, 62171081, 61901086), Singapore Ministry of Education (MOE) AcRF Tier 1 grants (RG157/23 & RT11/23), Singapore Agency for Science Technology and Research (A*STAR) (M24N7c0080 & H25-MRO3489), and Nanyang Assistant Professorship Start Up grant.

Author contributions

R.W. conceived the ideas, R.W. and Y.S. supervised the project, R.W., J.C., Z.Z., J.S., M.Z. and S.L. performed the theoretical modeling and numerical simulations, R.W. developed the experimental methods, R.W., J.C., Z.Z., J.S. and Z.Q. conducted the experimental measurements. R.W., Y.S., Y.L., B.Z.W and M.S.L. conducted data analysis. All authors wrote the manuscript and participated the discussions.

Conflict of interest

The authors declare no conflict of interests.

Data availability

All data supporting the findings of this study are provided in the paper and its Supplementary Information and will be deposited in a public repository after the manuscript is accepted.

Additional information

Supplementary information is available for this paper. Correspondence and requests for materials should be addressed to R.W.

Supplementary Files

This is a list of supplementary files associated with this preprint. Click to download.

- 20260703observationofsupertoroidalpulsesSM1.pdf